Impacts of Gravity Waves on Precipitation of Typhoon Nari (2001) at Landfall

Xiao-Dong Tang (唐曉東) and Ming-Jen Yang (楊明仁)

Department of Atmospheric Sciences

National Central University

Abstract

Mountain-induced gravity waves (MGWs) are found when typhoons impinge on rugged terrains. Convectively forced gravity waves (CGWs) can also be excited by deep convection within typhoons. During 0300-0500 UTC 18 September 2001, Typhoon Nari moved slowly across Taiwan with nearly-constant intensity. Morlet wavelet analysis is performed on the simulation result of Yang et al. (2008) with the 2-km horizontal grid size and 2-min data interval. Two dominant scales of GWs were found near Mt. Yushan. For the mountain-induced GW, it was relatively steady with the horizontal (vertical) wavelength of 90 (10) km. MGWs above Mt. Yushan resulted in abundant cloud water over the windward slope and little cloud water on the lee side. CGWs were sometimes produced and superposed upon the MGWs. Their ground-relative periods was about 23 minutes and horizontal (vertical) wavelength was 23 (6) km. CGWs consequently undulated wind, cloud water and surface rainfall at smaller spatial and temporal scales, compared to the MGWs.

1. Introduction

Observational studies and numerical simulations reveal that typhoon rainfalls on Taiwan are closely related to typhoon tracks and Taiwan's topography (Wu et al. 2002; Yang et al. 2008; Cheung et al. 2008). When airflows impinge steep mountain with appropriate Froude number, gravity waves (GWs) can be excited (Smith 1989). Mountain-induced GWs (MGWs) were found in landfalling typhoons as well as in other weather systems (Garvert et al. 2007; Fudeyasu et al 2008).

When typhoons moved across mountains, the seeder-feeder precipitation mechanism could contribute to surface rainfall enhancement; airflows induced by mountain waves could transfer precipitation particles to the lee side and low levels (Misumi 1996). GWs can be generated by deep convection within mesoscale convective systems (Yang and Houze 1995); convectively forced GWs (CGWs) would be expected in landfalling typhoons (Chagnon and Gray 2008).

The first objective of this study is to investigate essential features of MGWs and CGWs in Typhoon Nari (2001) over Taiwan, including their wavelengths, amplitudes, periods and dispersion relations, using the cloud-scale simulation results of Yang et al. (2008). The second objective is to examine how the relations among the GWs period, precipitation particles lifetime, and flow advection time scale across the mountain affect the rainfall distribution and accumulated amount. Through this diagnostic study, we wish to gain insight how the MGWs and CGWs interplay with precipitation for a landfalling typhoon.

2. Methodology

Morlet wavelet analysis is effective for analysis of geophysical phenomena. A full spectrum of coefficients can be calculated at each location in the spatial (or temporal) domain. It is better than the Fourier transform to isolate the spectral properties of a phenomenon that is

localized spatially or intermittent temporally. Detail of this method can be referred to Torrence and Compo (1998).

In this study, we have performed the Morlet wavelet analysis on the cloud-scale simulation results of Typhoon Nari by Yang et al. (2008) with the 2-km horizontal grid size and 2-min output interval, for the period of 0300-0500 UTC 18 September when the storm moved very slowly over southwestern Taiwan with nearly-constant intensity.

3. Results

It is clear from Fig. 1 and model animations that during 0300-0500 UTC 18 September 2001, convective cells were generated frequently and then moved downstream in the outer rainband region of Nari when the tangential flows impinged the Central Mountain Range (e.g. AA' in Fig. 1). Figure 2a exhibits the vertical velocity evolution of Point B on Line AA' at the altitude of 4 km during this 2-h period. The wavelet power spectra, or the coefficients of the wavelet transform multiplied by their conjugates, determined by the Morlet wavelet analysis of this vertical-velocity time series are shown in Fig. 2b. The spectra are contoured as a function of data time and oscillation period. Because this time series consists of data at 2-min intervals on a 2-km grid, signals with periods longer than 8 minutes are properly resolved. Only one maximum exists at each instant in the spectra, which is the wave period of approximately 23 minutes during this 2-h period. This is the dominant period for vertical velocity at Point B (in ground-relative framework), which will be verified as the CGW signal later.

Terrain heights along Line AA' are shown in Fig. 3a, and the corresponding wavelet power spectra for this terrain-height "spatial" series in Fig. 3b indicate the dominant wavelength at each position along Line AA'. There is only one maximum of the spectra for all points along the line, and they all correspond to the wavelength of nearly 90 km, which is the dominant wavelength for terrain heights along Line AA'.

Figure 4a shows the time-space plot (or Homöver diagram) of the vertical velocity at the altitude of 4 km MSL along Line AA' for the period of 0300-0500 UTC 18 September 2001. This diagram illustrates updraft/downdraft convective cells forced by the mountain and the associated gravity waves. The terrain height along cross section AA' rises steeply from 0.5 km to 2 km MSL near the position of 25 km (see Fig. 3a), where convective cells were triggered every 20-30 minutes. CGWs and MGWs were superimposed on each other, and the wavelengths for these two waves can be analyzed by wavelet analyses. The wavelet power spectra for the wavelengths of CGW and MGW can be obtained by performing the wavelet analysis of vertical velocity along cross section AA' at the 4-km altitude at a specific time, which can be every two minutes during 0300-0500 UTC 18 September; thus the evolution of wavelet power spectra of vertical velocity along cross section AA' is achieved. For example, Fig. 4b displays the evolution of wavelet power spectra of corresponding wavelengths of vertical velocity during the 2-h period at Point B along cross section AA' (cf. Fig. 1). There are two maxima of the spectra for most of the time and they correspond to two wavelengths of 23 km and 90 km, respectively (Fig. 4b). The wavelength of 90 km is consistent with that of terrain height along Line AA' (Fig. 3b), so the waves with 90-km wavelength are indeed MGWs. Along the windward slope between the horizontal distance of 20 and 60 km, updrafts arise persistently in the 2-h period (Figs. 3a and 4a). A standing lee wave occurs from the mountain peak to 15 km downstream (Fig. 4a). The downslope winds appear in the immediate lee, with maximum updrafts of more than 2 m s^{-1}. The waves with 23-km wavelength can be verified as CGWs from Fig. 4b, which are initially forced at the steep upslope (at 20 km along the "Distance" axis; see Fig. 3a) and then propagate downstream with the phase speed of 12 m s^{-1} (in

ground-relative framework).

Vertical motion has a close relation to cloud water mixing ratio for deep convection. Figure 5a exhibits the evolution of cloud-water mixing ratio at the same location during the same period as in Fig. 4a, and the evolution of its wavelet power spectra for cloud water at Point B is also shown in Fig. 5b. As expected intuitionally, a greater cloud-water mixing ratio generally occurs along the windward slope and a less mixing ratio is located on the lee side (it is smaller than 0.5 g kg^{-1} downstream from the mountain peak; see Fig. 5a). A high correlation exists between the cloud-water mixing ratio and vertical motion both spatially and temporally (cf Figs. 4a and 5a). The 90-km wavelength is also dominant in the analysis of wavelet power spectra for cloud-water mixing ratio (Fig. 5b). The secondary dominant wavelength for cloud-water mixing ratio is slightly longer than 23 km, which is the wavelength for CGWs in the analysis of vertical motion (Fig. 4b). It may be due to the horizontal advection of cloud water across mountain by Nari's tangential flows, thus increasing the horizontal wavelength for the variations of mass of cloud water.

Figure 6a is the height-time plot for the vertical velocity at Point C (see Fig. 1 for its location) during the 2-h period and Figure 6b shows the evolution of wavelet power spectra of corresponding vertical wavelengths for vertical velocity at the 7-km altitude. Most of the updraft cells extend to the altitude near 8 km, except for one developed at t = 70 min reaches to even higher levels (Fig. 6a). There are two dominant vertical wavelengths, 10 km and 6 km, respectively (Fig 6b). More analyses of vertical structure for updrafts at other points suggest that the 6-km-wavelength mode only exists when strong convective updraft cells occur with few updraft cells aloft, while the 10-km-wavelength mode can exists without precipitation (figure not shown). Therefore it can be deduced that the mode with vertical wavelength of 6 km points to the CGWs, while the mode with vertical wavelength of 10 km points to the MGWs. More detailed discussion will be given during the oral presentation in the conference.

References

Chagnon, J. M. and S. L. Gray, 2008: Analysis of convectively-generated gravity waves in mesoscale model simulations and wind-profiler observations. *Quart. J. Roy. Meteor. Soc.*, **134**, 663–676.

Cheung, K. K. W., L.-R. Huang, and C.-S. Lee, 2008: Characteristics of rainfall during tropical cyclone periods in Taiwan. *Nat. Hazards Earth Syst. Sci.*, **8**, 1463–1474.

Fudeyasu, H., T. Kuwagata, Y. Ohashi, S.-I. Suzuki, Y. Kiyohara, and Y. Hozumi., 2008: Numerical study of the local downslope wind "Hirodo-kaze" in Japan. *Mon. Wea. Rev.* **136**, 27-40.

Garvert, M. F., B. Smull, and C. Mass, 2007: Multiscale mountain waves influencing a major orographic precipitation event. *J. Atmos. Sci.*, **64**, 711-737.

Misumi, R., 1996: A study of the heavy rainfall over the Ohsumi Peninsula (Japan) caused by typhoon 9307. *J. Meteor. Soc. Japan.* **74**, 101-113.

Smith, R. B., 1989: Hydrostatic airflow over mountains. *Advances in Geophysics*, Vol. 31, Academic Press, 1–41.

Torrence, C., and G. P. Compo, 1998: A practical guide to wavelet analysis. *Bull. Amer. Meteor. Soc.*, **79**, 61–78.

Yang, M.-J., and R. A. Houze, Jr., 1995: Multicell squall line structure as a manifestation of vertically trapped gravity waves. *Mon. Wea. Rev.*, **123**, 641-661.

Yang, M.-J., D.-L. Zhang, and H.-L. Huang, 2008: A modeling study of Typhoon Nari (2001) at landfall. Part I: The topographic effects. *J. Atmos. Sci.*, **65**, 3095-3115

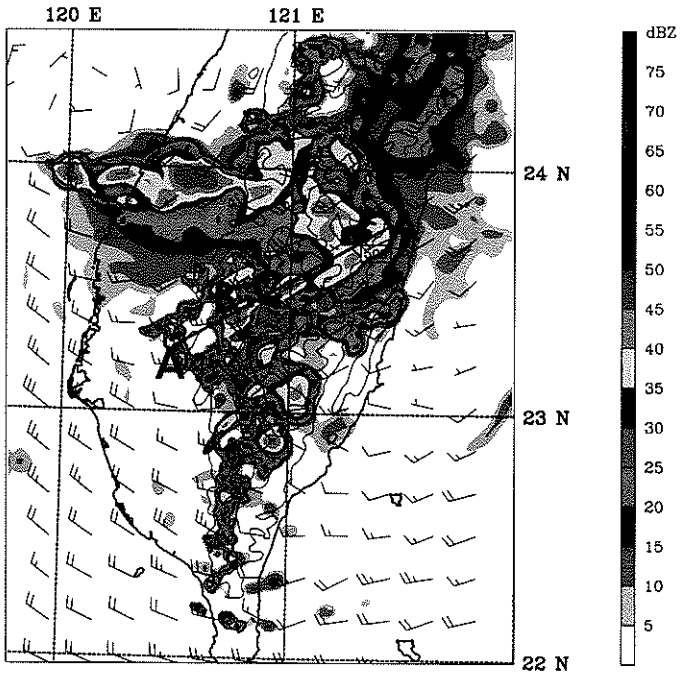

Figure 1: A composite of vertical maximum radar reflectivity (colored) and horizontal wind barbs at the 4-km level at 0400 UTC 18 Sept 2001, superposed with terrain height (thin solid) at 1000-m interval (starting from the 500-m height). Line AA' denotes the location of vertical cross section, along which two points B and C are located.

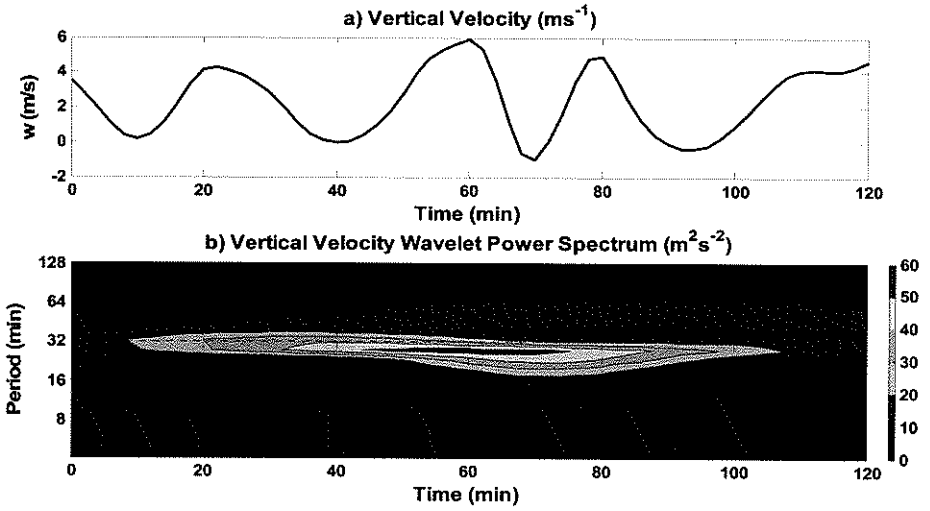

Figure 2: (a) Time series of vertical velocity (W; in units of m s^{-1}) at Point B at the 4-km level taken in Fig. 1 during 0300-0500 UTC 18 Sept 2001. (b) Corresponding Morlet wavelet analysis.

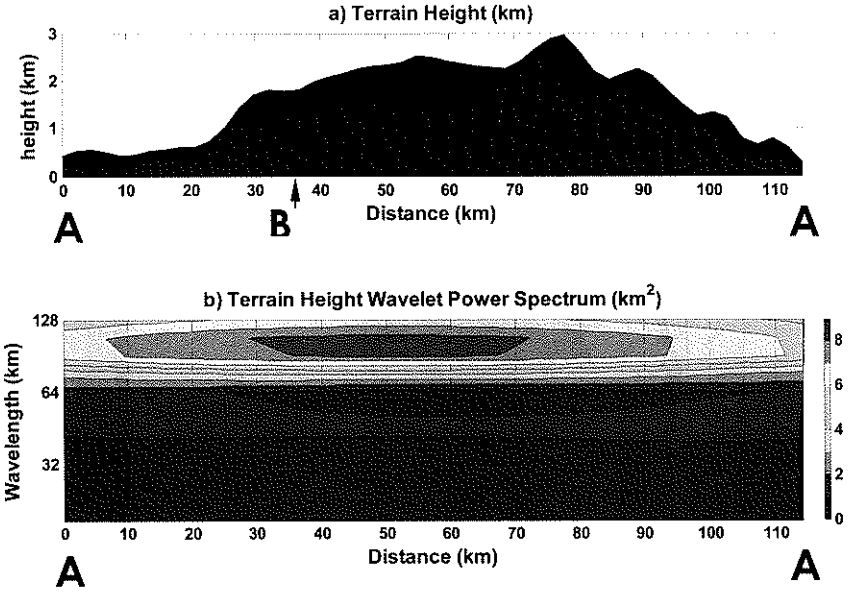

Figure 3: (a) Terrain height (in unit of km) along Line AA' in Fig. 1. (b) Corresponding Morlet wavelet analysis. The arrow in (a) denotes the position of Point B in Fig. 1.

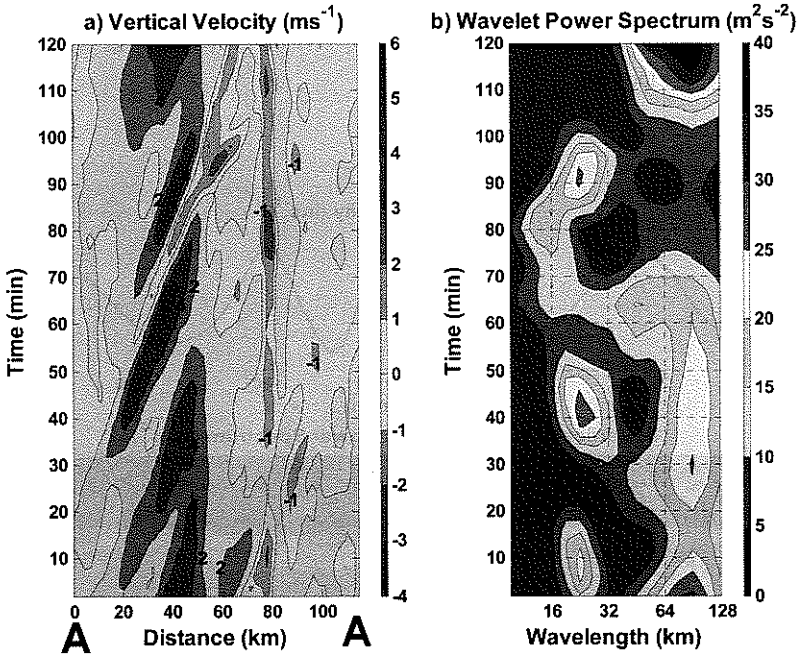

Figure 4: (a) Time-space plot of vertical velocity along Line AA' in Fig. 1 at the 4-km level during 0300-0500 UTC 18 Sept 2001, contoured at -2, -1, 0, 2, 4, and 6 m s^{-1}, respectively. (b) Corresponding Morlet wavelet analysis for the horizontal structure of vertical velocity at Point B.

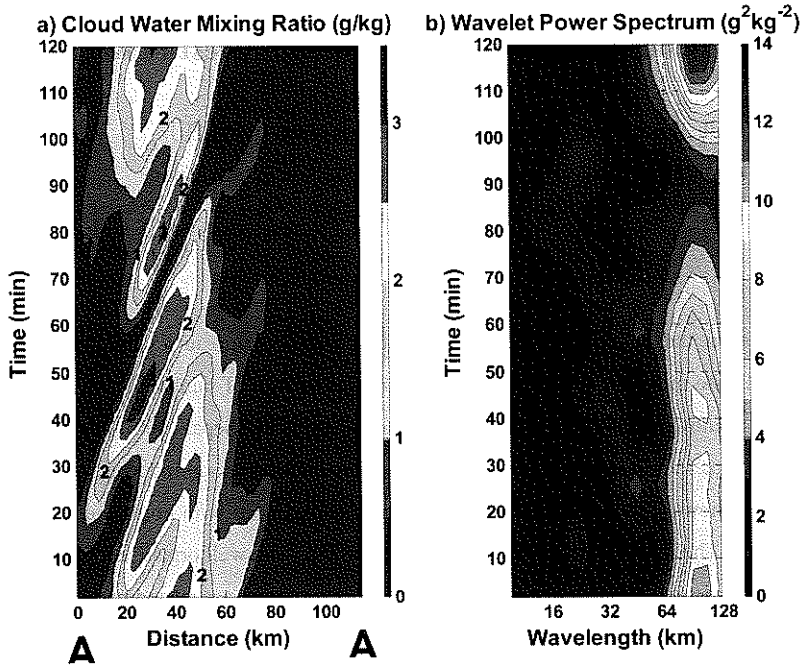

Figure 5: As in Fig. 4 but for the cloud-water mixing ratio.

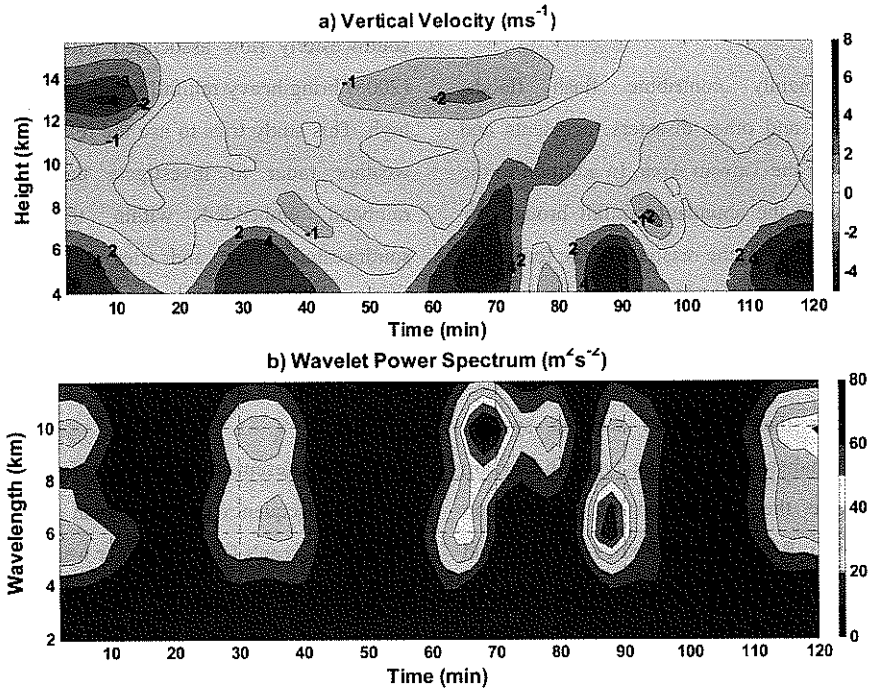

Figure 6. (a) Height-time plot of vertical velocity at Point C in Fig. 1 during 0300-0500 UTC 18 Sept 2001. (b) Corresponding Morlet wavelet analysis for the vertical structure of vertical velocity at the 7-km level.